J Mater Sci (2011) 46:4606–4613
DOI 10.1007/s10853-011-5360-8

Controllable synthesis of hexagonal close-packed nickel nanoparticles under high nickel concentration and its catalytic properties

Yong Guo · Muhammad Usman Azmat · Xiaohui Liu · Jiawen Ren · Yanqin Wang · Guanzhong Lu

Received: 4 January 2011 / Accepted: 31 January 2011 / Published online: 12 February 2011

Abstract The hexagonal close-packed (hcp) Ni nanoparticles have been synthesized successfully in triethylene glycol with high ionic Ni concentration under the presence of protective agent (PVP or PEG). The protective agent (PVP or PEG) played an important role in the formation of hcp Ni. The crystal structure of nickel can be tuned by changing the concentration of Ni ions, reaction temperature, and amount of protectors. The X-ray diffraction and magnetic studies revealed the formation of pure hcp Ni. The VSM study showed that the magnetic properties of hcp Ni is quite different from that of face-centered cubic (fcc) Ni. The hcp Ni nanoparticle had a low saturation magnetization, while the coercivity value of hcp Ni was nearly the same as that of fcc Ni. A stable hcp Ni supported on γ-Al_2O_3 catalyst was also prepared successfully for the first time and its catalytic activity was investigated in the aqueous-phase reforming of glycerol. The achieved conversion of glycerol and selectivity to hydrogen was high up to 52 and 64%, while the selectivity to methane was only 5%, indicating the preventing of methanation on hcp Ni.

Introduction

Nanostructured magnetic particles have received considerable attention because of their crucial application in the fields of catalysis [1–4], high-density magnetic storage devices [5], magnetic sensors [6], and magnetic carriers for drug targeting [7]. Among these magnetic particles, Ni nanoparticles (NPs) have attracted much attention and been investigated intensely. Ni has two typical crystallographic phases: face-centered cubic (fcc), and hexagonal close-packed (hcp) phases. Naturally, Ni crystallizes as fcc structure with ferromagnetic properties. Fcc Ni NPs have been synthesized through a couple of methods [8–11].

The hcp Ni is considered as a metastable phase, which can be observed only in thin films under specific preparations [12, 13]. Though the information about hcp Ni NPs are rare, the synthesis and characterization of hcp Ni have attracted widespread attention. In the last decade, several groups have prepared hcp Ni NPs using different techniques and their magnetic properties were also studied [14–24]. In these methods, polyol process is comparatively easy and reliable, but it is only suitable for the synthesis at low Ni^{2+} concentration (0.0025 M Ni^{2+}) [15]. As far as our knowledge is concerned, there was no report on the synthesis at relatively high Ni^{2+} concentration, and the catalytic properties of hcp Ni NPs have never been reported.

In this study, we report a one-pot chemical route for controllable synthesis of fcc and hcp Ni NPs by a polyol process. Hcp Ni NPs were prepared successfully in triethylene glycol (TEG) with a higher concentration of Ni^{2+} under the assistance of polyvinylpyrrolidone (PVP M_w = 40000) or polyethylene glycol (PEG M_w = 20000). Besides, stable hcp Ni NPs supported on γ-Al_2O_3 catalyst, which was named as HN was also synthesized in situ and used as a catalyst in the production of hydrogen by the aqueous-phase reforming (APR) of glycerol. It showed high selectivity to H_2 and low selectivity to methane, indicating it can prevent methanation.

Y. Guo · M. U. Azmat · X. Liu · J. Ren · Y. Wang (✉) · G. Lu (✉)
Key Lab for Advanced Materials, Research Institute of Industrial Catalysis, East China University of Science and Technology, Shanghai 200237, People's Republic of China
e-mail: wangyanqin@ecust.edu.cn

G. Lu
e-mail: gzhlu@ecust.edu.cn

Experimental section

Synthesis of hcp Ni NPs and hcp Ni NPs supported γ-Al_2O_3 catalyst (HN)

The Ni NPs were synthesized from nickel(II) acetate tetrahydrate ($Ni(CH_3COO)_2{\cdot}4H_2O$) in triethylene glycol (TEG). Calculated amount of $Ni(CH_3COO)_2{\cdot}4H_2O$ and protective agent (PVP or PEG) were added to 100 mL of TEG in a three-neck flask and treated ultrasonically for 30 min to dissolve the metal precursors and polymer. Then, the solution was refluxed at certain temperature in a sand or oil bath for 3 h under gentle mechanical stirring. During reaction, a nitrogen flow was passed through the system to take away air and moisture. After reaction, the system was cooled down to room temperature. The products were obtained by centrifugation, and then washed with water and absolute ethanol to remove impurities. Finally, the washed black powder was dried in a vacuum oven overnight. The Ni^{2+} concentration, reaction temperature, and protective agent were changed, and the results are summarized in Table 1.

For the synthesis of hcp Ni NP-supported γ-Al_2O_3 catalyst (HN), calculated amount of γ-Al_2O_3 was added into the above solution and ultrasonicated for 5 min before refluxing. The other procedures were the same as those for hcp Ni NPs. After drying in vacuum oven, the product was annealed at 573 K in nitrogen atmosphere for 4 h. The fcc Ni NP-supported γ-Al_2O_3 catalyst (FN) was obtained by annealing the HN catalyst at 673 K in nitrogen atmosphere for 4 h.

Characterization

The powder X-ray diffraction (XRD) patterns were obtained on a Bruker AXS D8 Advance X-ray diffractometer (Cu Kα radiation, $\lambda = 1.5406$ Å), operated at 40 kV and 40 mA, respectively. The compositions of the catalysts were determined by inductively coupled plasma-atomic emission spectrometry (ICP-AES) on an IRIS Intrepid spectrometer. Transmission electron microscope (TEM) images were obtained using FEI Tecnai 20 S-TWIN operating at 200 kV. Scanning electron microscopy (SEM) images were performed on a HITACHI S-3400 N scanning electron microscope operating at an acceleration voltage of 15 kV. Magnetic properties of the samples were recorded using the vibrating sample magnetometer (VSM, Lakeshore, Model 7407) measurement. BET surface areas were measured at 77 K on a NOVA 4200e surface area and pore-size analyzer. Before the measurements, the samples were outgassed at 180°C in vacuum for 6 h.

Activity test

The activity test was performed by APR of glycerol in a fixed bed reactor system. The catalysts were pelletized and sieved to 40–60 mesh size. Then, 1.0 g of catalyst was loaded in the stainless steel tubular reactor with an inner diameter of 6 mm. 1 wt% of glycerol was fed into the reactor at a flow rate of 3.6 mL/h by an HPLC pump. The reforming was conducted at 498 K and 2.76 MPa. Gaseous products were analyzed using an on-line gas chromatograph equipped with FID and TCD detectors and a methanizer.

Results and discussion

Phase composition and magnetic studies

Figure 1 shows the XRD patterns of samples (a)–(e) synthesized in the absence of protective agent. Samples (a)–(c) were synthesized at 563 K with 0.0025, 0.005, and 0.02 M Ni^{2+}, respectively. The diffraction peaks at 2θ of

Table 1 Reaction conditions and results for the synthesis of Ni nanoparticles

Sample	Ni^{2+} concentration (M)	Protective agent	Temperature (K)	Phase
(a)	0.0025	No	563	hcp
(b)	0.005	No	563	hcp
(c)	0.02	No	563	fcc + hcp
(d)	0.02	No	473	fcc + hcp
(e)	0.02	No	453	fcc
(f)	0.02	1.00 g PVP	563	hcp
(g)	0.02	0.42 g PEG	563	hcp
(h)	0.03	1.00 g PVP	563	fcc + hcp
(i)	0.03	1.50 g PVP	563	hcp
(j)	0.04	1.00 g PVP	563	fcc + hcp
(k)	0.04	2.00 g PVP	563	fcc + hcp
(l)	0.04	4.00 g PVP	563	hcp

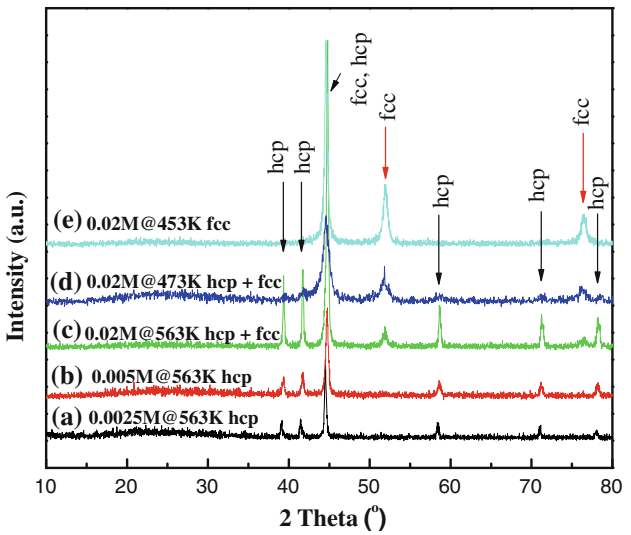

Fig. 1 XRD patterns of Ni NPs synthesized with different Ni^{2+} concentration at various temperature without protective agent

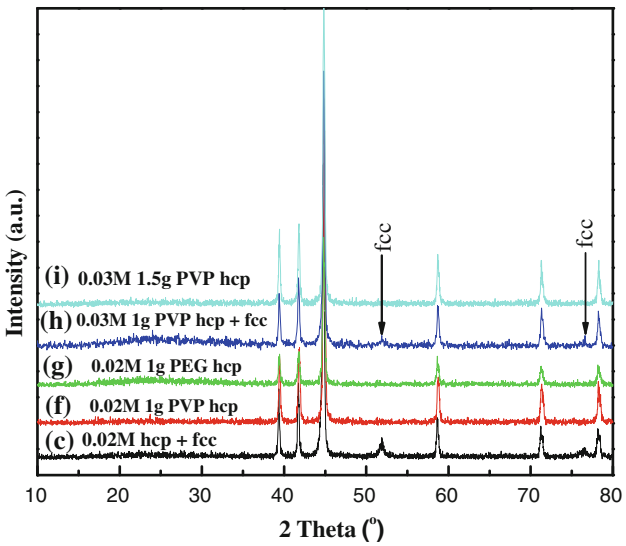

Fig. 2 XRD patterns of Ni NPs synthesized at 563 K with different concentrations of Ni^{2+} and protective agent

39.1°, 41.5°, 44.5°, 58.5°, 71.1°, and 78.0° in Fig. 1a and b are assigned to (010), (002), (011), (012), (110), and (103) planes of hcp Ni (JCPDS card No. 45-1027). In these two patterns, no peaks of fcc Ni or Ni-oxide were observed, indicating that the nanoparticles obtained have a pure hcp phase. In Fig. 1c, on the other hand, the peaks at 2θ of 52.0°, and 76.4° assigned to, respectively, (200) and (220) planes of fcc Ni (JCPDS No. 04-0850) are observed, indicating that the mixture of fcc Ni and hcp Ni was obtained at high Ni^{2+} concentration (0.02 M). It should be noted that the main peak (111) of fcc Ni overlaps with that of the hcp Ni (011). Samples (c), (d), and (e) were synthesized with 0.02 M of Ni^{2+} at 563, 473, and 453 K, respectively. Samples (c) and (d) were the mixture of fcc and hcp Ni, while sample (e) was a pure fcc Ni. These results indicate that high reaction temperature and low concentration of Ni^{2+} prefer the formation of hcp Ni. This is in agreement with Chinnasamy's [15] and Mourdikoudis's studies [24].

Figure 2 depicts the XRD patterns of samples (c) and (f)–(i). Samples (f) and (g) were synthesized with 0.02 M Ni^{2+} at 563 K, but with 1.0 g of PVP or PEG as the protective agent, respectively. It can be seen from the XRD patterns that only the peaks of pure hcp phase Ni appeared, which can be assumed that the protective agent (PVP or PEG) plays a very important role in the formation of hcp Ni. PVP has proved to be a useful protecting polymer and could protect almost all kinds of NPs in various systems [25], and so it was chosen as the protective agent in the following process. In order to prove the effect of PVP, a series of Ni NPs were synthesized under the assistance of PVP. Sample (h) and (i) were synthesized with 0.03 M Ni^{2+} at 563 K, with 1.0 and 1.5 g PVP, respectively. According to the XRD patterns, pure hcp Ni NPs were formed for sample (i), while it is a mixture of fcc and hcp Ni NPs for sample (h). This means that more PVP needed to form pure hcp Ni NPs at high Ni concentration. When the Ni^{2+} concentration was increased to 0.04 M, a mixture of fcc and hcp phase Ni was obtained when 1.5 or 2.0 g PVP was added, but on further increasing the amount of PVP to 4 g, a pure hcp phase was obtained again (Fig. 3).

The unit cell parameters of the synthesized samples of pure hcp or fcc phase Ni are summarized in Table 2. All of the parameters were calculated according to the XRD patterns. The unit cell parameters of sample (e) (fcc phase) are estimated to be $a = 0.3519$ nm, which are similar with

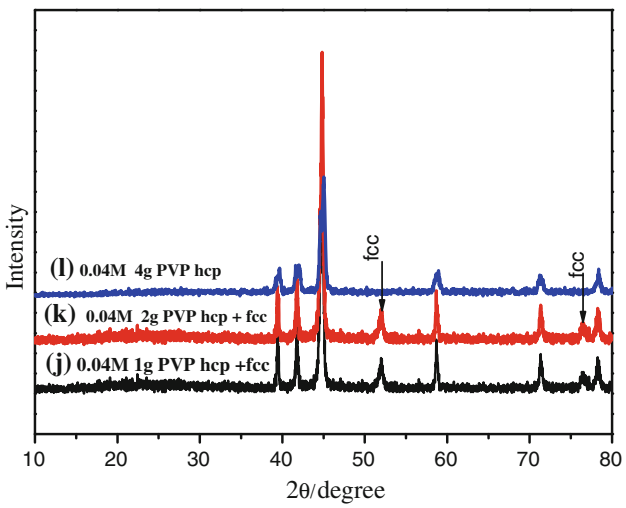

Fig. 3 XRD patterns of mixture of fcc and hcp phase Ni NPs synthesized with 0.04 M concentration of Ni^{2+} and different concentrations of PVP at 563 K

Table 2 The unit cell parameters and crystallite sizes of hcp and fcc Ni NPs synthesized in different conditions

Sample	Phase	*a* (nm)	*c* (nm)	*c*/*a*	Size (nm)
(a)	hcp	0.2660	0.4339	1.631	29.3
(b)	hcp	0.2642	0.4345	1.645	23.8
(c)	fcc + hcp	–	–	–	13.2/24.1[a]
(d)	fcc + hcp	–	–	–	9.3/–
(e)	fcc	0.3519	0.3519	1	11.4
(f)	hcp	0.2639	0.4326	1.639	27.6
(g)	hcp	0.2641	0.4330	1.639	24.4
(h)	fcc + hcp	–	–	–	–/32.3
(i)	hcp	0.2639	0.4329	1.641	35.3
(j)	fcc + hcp	–	–	–	17.6/25.4
(k)	fcc + hcp	–	–	–	21.3/27.2

[a] crystallite sizes calculated according to fcc and hcp phase, respectively

that in the literature [24, 26]. The cell parameters of all of the hcp Ni synthesized in this study are similar with each other, having $a \approx 0.264$ nm and c is 0.433 nm, which is much close to many references on hcp Ni [16–18, 21, 23, 24, 27, 28]. The calculated c/a values for the synthesized samples of hcp Ni are around 1.63, which is a characteristic of a close-packed arrangement [23].

The crystallite sizes of the samples derived from the (110) reflection for hcp or (200) for fcc can be calculated by the Scherrer equation and are shown in Table 2. The average crystallite sizes of pure hcp Ni are larger than that of pure fcc or mixture of fcc and hcp Ni.

The representative morphologies and sizes of Ni NPs are observed using SEM/TEM and shown in Figs. 4 and 5, respectively. In sample (c) (Fig. 4a), both spheres and plates agglomerated by the spheres are co-existing, and the corresponding TEM image (Fig. 5a) shows that the particle size is in the range of 150–500 nm. The addition of PVP in sample (f) and (k) (Fig. 4c, d) resulted in the formation of the well-dispersed spheres, but their surfaces were rough. However, from the TEM images (Fig. 5c, d), the distribution of the particle size was uniform in sample (f) relative to that in sample (k). The average size of spheres was ca. 200 nm in sample (f), while the size was distributed from 100 to 500 nm in sample (k). Besides, Fig. 5c shows that the spheres seem to be formed by some sheets overlapped with each other in sample (f). In sample (e), only agglomeration was found as shown in Fig. 4b. Thus, it is proposed that hcp Ni is favored to exist in the form of the spheres enclosed by sheets overlapping, and the presence of PVP promotes the formation of hcp Ni. Remarkably, the size of the spheres shown in SEM or TEM did not agree with that obtained from XRD, which may indicate that the larger spheres in these samples are composed of smaller crystallites.

Aiming to investigate the magnetic properties of the as-synthesized Ni NPs, the hysteresis loops at room temperature were recorded. The magnetic properties of the synthesized samples under different conditions are summarized in Table 3. The magnetization values were normalized to magnetization/mass of sample (emu g^{-1}).

Figure 6 shows the hysteresis loops of Ni NPs synthesized at different temperatures. The saturation magnetization

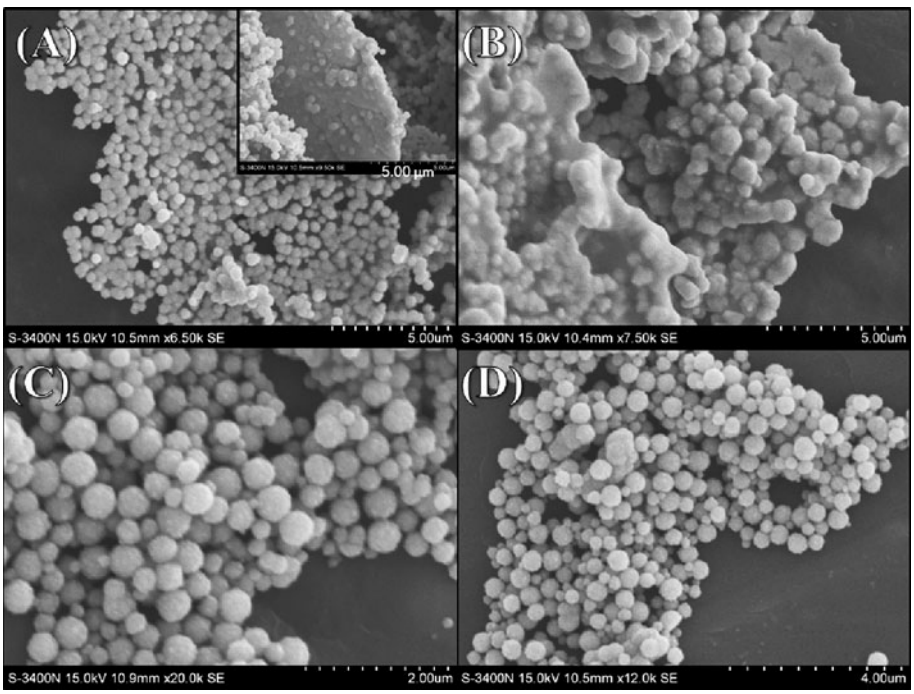

Fig. 4 SEM image of sample (c) (**a**); (e) (**b**); (f) (**c**), and (k) (**d**)

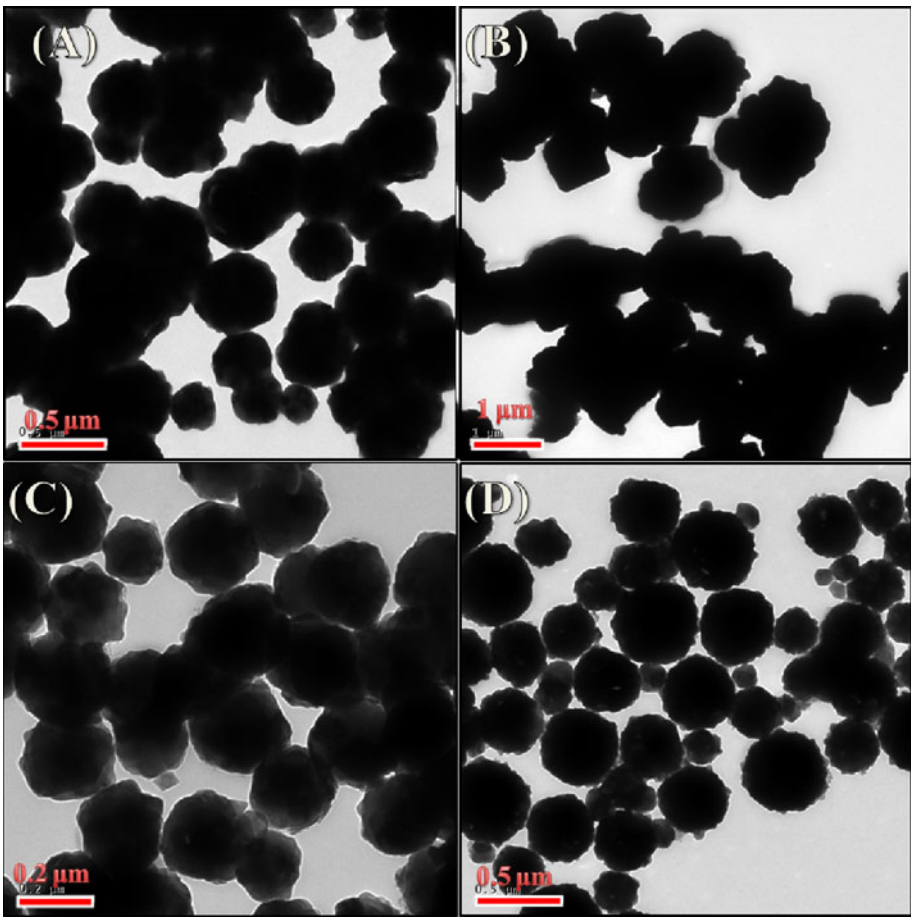

Fig. 5 TEM image of sample (c) (**a**); (e) (**b**); (f) (**c**), and (k) (**d**)

(M_s), remnant magnetization (M_r), and coercivity (H_c) are increased gradually by decreasing the reaction temperature for the samples (c)–(e). As previously mentioned in the XRD patterns, pure fcc Ni has the highest M_s value, 31.55 emu g^{-1}. The samples containing a fraction of hcp Ni shows lower M_s values than pure fcc Ni sample. Though theoretically, the hcp Ni was predicted to be strongly ferromagnetic [29], experimental proof by different researchers [17–19, 23, 30], however, differs from the theoretical studies, showing that the M_s of hcp Ni is much lower than the value expected. Thus, according to the XRD patterns and the magnetic properties, we may conclude that Ni NPs synthesized at high temperature contains a greater fraction of hcp Ni, which suggests that high temperature is favored for the formation of hcp Ni.

Samples (f) and (g) show extremely low M_s values, while the H_c values are nearly the same as those in fcc Ni. As mentioned with respect to the XRD patterns, the protective agent is necessary to synthesize the hcp Ni under high concentration of precursor. Considering the magnetic properties of samples (f), (i), and (k) in Table 3, the M_s value increased as the concentration of Ni was increased, indicating that the number of fcc Ni NPs increased with increasing concentration of Ni^{2+}.

Table 3 The magnetic properties of the as-synthesized samples under different conditions

Sample	Phase	M_s (emu g^{-1})	M_r (emu g^{-1})	H_c (Oe)
(c)	fcc + hcp	7.85	1.45	156
(d)	fcc + hcp	16.47	2.98	181
(e)	fcc	31.55	5.40	191
(f)	hcp	0.120	0.038	207
(g)	hcp	0.085	0.018	162
(i)	hcp	0.440	0.131	205
(k)	fcc + hcp	10.00	2.32	192

All the above data demonstrate that the magnetic properties of fcc Ni NPs are stronger than that of hcp Ni NPs. The primary particle size is considered to play a decisive role on the crystallite structure of Ni NPs [15]. By increasing the reaction kinetics, the particle size of Ni was reduced, and the structure was changed from fcc phase to hcp phase [14]. In this study, we proposed a possible mechanism for the formation of hcp NPs (see Scheme 1). Initially, it rapidly formed smaller nucleus at low concentration of Ni precursor and high temperature. Then, the small nucleus arranges to form hcp phase Ni NPs. While considering the formation of

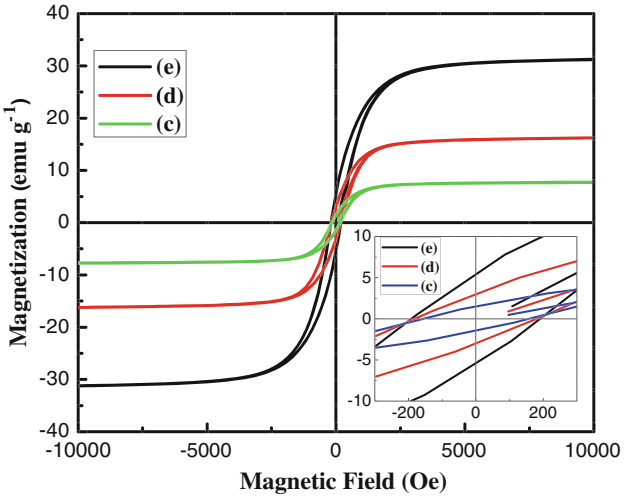

Fig. 6 Hysteresis loops of sample (c), (d), and (e) at 300 K. The insets show the low field details of the cycles

pure hcp Ni NPs with high concentration of Ni precursor in the presence of protector, one reasonable explanation is that PVP or PEG inhibits the growth of nucleus after nucleating and promotes arrangement of small nucleus.

Catalytic activity

Hydrogen production through APR process has been studied widely as it can produce hydrogen with extremely low CO content while using low-cost, renewable oxygenated hydrocarbons derived from biomass that are environmentally benign [31–33]. Ni-based catalyst is much cheaper than Pt-based catalyst and has been proved to be an effective catalyst for APR [1, 2], but Ni-based catalyst promoted the methanation in the process of APR, which caused the decrease of the hydrogen selectivity. Thus, it is necessary to promote the selectivity to hydrogen on Ni-based catalyst. In order to investigate the catalytic properties of hcp Ni NPs, APR of glycerol was carried out in this study.

Table 4 shows the catalytic performance for APR of 1.0 wt% glycerol on FN (fcc Ni on Al_2O_3) and HN (hcp Ni on Al_2O_3) catalysts. Although the conversion was 29% on the 10-HN catalyst, which is just a little higher than that on 10-FN catalyst (25%), but the selectivity to hydrogen on 10-HN was 77%, which is quite higher than that on 10-FN catalyst (63%). Compared with the supported fcc Ni catalyst with 20% loading reported by A. Iriondo et al. [34], the 20-HN catalyst exhibited a relative higher activity. The conversion and selectivity to hydrogen achieved were up to 52 and 64%, respectively. Additionally, the selectivity to methane on all of the three catalysts was very low. It is assumed that the hcp Ni may be helpful towards producing hydrogen and inhibiting methanation in the APR process of glycerol. Based on density functional theory calculation and experiments, Bengarrd et al. [35] identified that steam reforming of methane over Ni catalysts was extremely structure sensitive-step as Ni (211) surface was considered more reactive. In hcp Ni, maybe more Ni (211) surface was exposed.

Characteristics of the catalysts used in this study are summarized in Table 5. The loading amounts of Ni were found to be lower than the calculated data. All the three catalysts have almost the same BET surface area. Synthesized HN catalysts show the characteristics peaks of hcp Ni in the XRD patterns (see Fig. 7), and the peak broadening is also observed compared to the pure hcp Ni NPs synthesized previously, indicating that smaller Ni crystallite was obtained in presence of γ-Al_2O_3. FN catalyst was prepared by annealing the product at 673 K in nitrogen for 4 h, and fcc phase Ni was obtained. This agreed with literature [16], wherein it is reported that hcp Ni underwent a transition to an fcc phase above 653 K. The XRD patterns

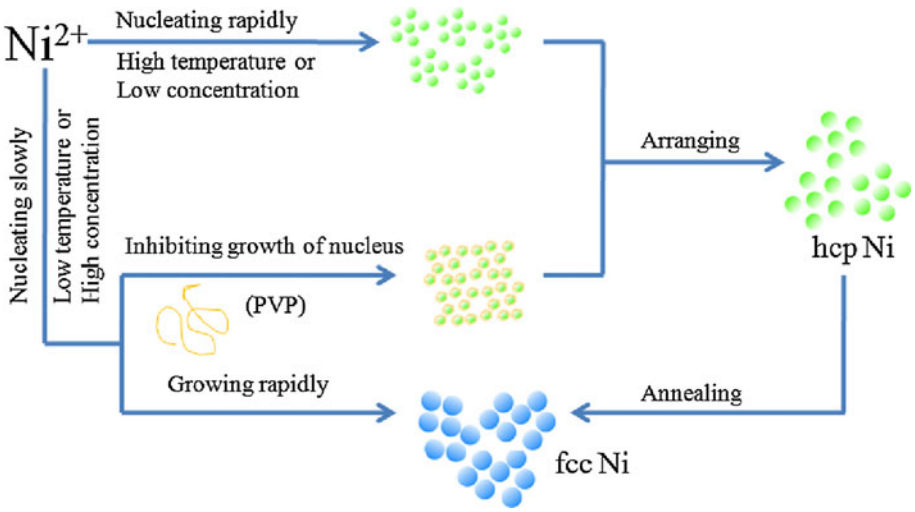

Scheme 1 Proposed mechanism of formation of hcp and fcc Ni NPs

Table 4 Catalytic performance for APR of 1 wt% glycerol on FN and HN catalysts at 498 K, 2.76 MPa, flow rate of 0.06 mL/min, and 40 h on stream

Catalyst	Conc. of C to gas (%)	Gas products[a] (mol%)				Selectivity[b] (%)		Yield of H_2 (%)
		H_2	CO_2	CO	CH_4	H_2	CH_4	
10-FN[c]	25	59.7	38.9	0.7	0.7	63	2	16
10-HN	29	64.3	34.1	0.6	1.0	77	3	22
20-HN	52	59.8	37.9	0.2	2.1	64	5	33
20-FN[d]	36	32	42	–	26	–	–	–

[a] no C_{2+} alkanes were detected

[b] H_2 selectivity = (molecules of H_2 produced/C atoms in gas phase) × (1/R) × 100%, where R = 7/3

CH_4 selectivity = (C atoms in gaseous alkanes/total C atoms in gas-phase product) × 100%. It should be indicated that H_2 and alkane selectivities do not add to 100%, because they are calculated based on the independent H and C balances, respectively

[c] 10 Means the theoretic load amount of Ni is 10 wt%

[d] The data from the literature [34]

Table 5 Physical properties of the catalysts

Catalyst	Ni content[a] (wt%)	S_{BET} (m^2 g^{-1})	d^b_{Ni} (nm)
10-FN	7.9	160.3	18
10-HN	7.9	158.5	15
20-HN	17	158.0	14

[a] Determined by ICP-AES

[b] Ni crystallite size determined by XRD

of the used 20-HN catalyst displayed obvious diffraction peaks of hcp Ni, indicating that there was no phase transition during the pelletizing in the pressure of 10 MPa and the APR process. In other words, the hcp Ni phase is tolerant enough at high pressures.

Conclusions

The hcp Ni NPs have been synthesized successfully under different reaction conditions via a simple and reliable one-pot reaction. Pure hcp Ni NPs are obtained even for 0.03 M Ni^{2+} using cheap acetate tetrahydrate nickle as a precursor, PVP as a protective agent, and triethylene glycol as a reducing agent. The concentration of Ni precursor and the reaction temperature are found to influence the structure of Ni NPs. Low Ni^{2+} concentration and high reaction temperature are favorable to form the hcp Ni NPs or vice versa. PVP (or PEG) plays a necessary role in synthesizing pure hcp Ni NPs with high concentration of Ni precursor through controlling the primary particle size. All the pure hcp Ni NPs show extremely low saturation magnetization and remnant magnetization values, while the magnetic coercivity of them are nearly the same as that of fcc Ni NPs. The catalysts of hcp Ni supported on γ-Al_2O_3 are stable at temperature of ca. 500 K and a high pressure of ca. 10 MPa. The catalysts exhibit high activity for APR of glycerol to produce hydrogen. The highest conversion achieved is up to 52% with selectivity to hydrogen and methane being 64 and 5%, respectively.

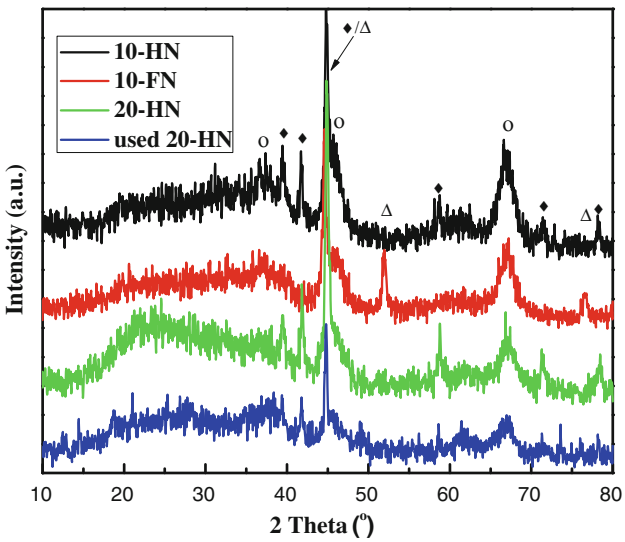

Fig. 7 The XRD patterns of the as-prepared catalysts and used 20-HN catalyst. (*open triangle*) fcc Ni; (*filled diamond*) hcp Ni; (*open circle*) γ-Al_2O_3

Acknowledgements This project was supported financially by the 973 Program of China (2010CB732300), the National Natural Science Foundation of China (No. 20973058), the Commission of Science and Technology of Shanghai Municipality (10XD1401400), and the "Excellent scholarship" of East China University of Science and Technology, China.

References

1. Huber GW, Shabaker JW, Dumesic JA (2003) Science 300:2075
2. Zhu LJ, Guo PJ, Chu XW, Yan SR, Qiao MH, Fan KN, Zhang XX, Zong BN (2008) Green Chem 10:1323
3. Wu ZJ, Zhang MH, Zhao ZF, Li W, Tao KY (2008) J Catal 256:323

4. Li HX, Zhao QF, Wan Y, Dai WL, Qiao MH (2006) J Catal 244:251
5. Jung SW, Park WI, Yi GC, Kim M (2003) Adv Mater 15:1358
6. Wang SF, Xie F, Hu RF (2007) Sensor Actuator B Chem 123:495
7. Zhang RY, Wang XM, Wu CH, Song M, Li JY, Lv G, Zhou J, Chen C, Dai YY, Gao F, Fu DG, Li XO, Guan ZQ, Chen BA (2006) Nanotechnology 17:3622
8. Hou Y, Gao S (2003) J Mater Chem 13:1510
9. Wu SH, Chen DH (2003) J Colloid Interface Sci 259:282
10. Park J, Kang E, Son SU, Park HM, Lee MK, Kim J, Kim KW, Noh HJ, Park JH, Bae CJ, Park JG, Hyeon T (2005) Adv Mater 17:429
11. Cordente N, Respaud M, Senocq F, Casanove MJ, Amiens C, Chaudret B (2001) Nano Lett 1:565
12. Zharkov SM, Zhigalov VS, Frolov GI (1996) Phys Met Metallogr 81:328
13. Tuaillon J, Dupuis V, Melinin P, Prevel B, Treilleux M, Perez A, Pellarin M, Vialle JL, Royer M (1997) Philos Mag A 76:493
14. Hinotsu T, Jeyadevan B, Chinnasamy CN, Shinoda K, Tohji K (2004) J Appl Phys 5:7477
15. Chinnasamy CN, Jeyadevan B, Shinoda K, Tohji K, Narayanasamy A, Sato K, Hisano S (2005) J Appl Phys 97: 10J309
16. Mi YZ, Yuan DS, Liu YL, Zhang JX, Xiao Y (2005) Mater Chem Phys 89:359
17. Tzitzios V, Basina G, Gjoka M, Alexandrakis V, Georgakilas V, Niarchos D, Boukos N, Petridis D (2006) Nanotechnology 17:3750
18. Jeon YT, Moon JY, Lee GH, Park J, Chang Y (2006) J Phys Chem B 110:1187
19. Han M, Liu Q, He JH, Song Y, Xu Z, Zhu JM (2007) Adv Mater 19:1096
20. Mireille RP, Murielle G, Serge V, Cédric L, Claude E, Mohamedally K (2007) Chem Mater 19:865
21. Gong J, Wang LL, Liu Y, Yang JH, Zong ZG (2008) J Alloy Compd 457:6
22. Yang JH, Feng B, Liu Y, Zhang YJ, Yang LL, Wang YX, Wei MB, Lang JH, Wang DD (2009) J Alloy Compd 467:L21
23. Luo XH, Chen YZ, Yue GH, Peng DL, Luo XT (2009) J Alloy Compd 476:864
24. Mourdikoudis S, Simeonidis D, Vilalta-Clemente A, Tuna F, Tsiaoussis I, Angelakeris M, Dendrinou-Samara C, Kalogirou O (2009) J Magn Magn Mater 321:2723
25. Toshima N, Yan H, Shiraishi Y (2008) Metal nanoclusters in catalysis and materials science: the issue of size control. Elsevier, Amsterdam
26. Gong J, Liu Y, Wang LL, Yang JH, Zong ZG (2008) Front Chem China 3:157
27. Vergara J, Madurga V (2002) J Mater Res 17:2099
28. Syukri BT, Ohya Y, Takahashi Y (2003) Mater Chem Phys 78:645
29. He X, Kong LT, Liu BX (2005) J Appl Phys 97:106107
30. Tian F, Zhu J, Wei D (2007) J Phys Chem C 111:6994
31. Cortright RD, Davda RR, Dumesic JA (2002) Nature 418:64
32. Davda RR, Dumesic JA (2003) Angew Chem Int Ed 42:4068
33. Davda RR, Dumesic JA (2004) Chem Commun 1:36
34. Iriondo A, Barrio VL, Cambra JF, Arias PL, Güemez MB, Navarro RM, Sánchez-Sánchez MC, Fierro JLG (2008) Top Catal 49:46
35. Bengaard HS, Nørskov JK, Sehested J, Clausen BS, Nielsen LP, Molenbroek AM, Rostrup-Nielsen JR (2002) J Catal 209:365